Ref. Ares(2022)7255761 – 19/10/2022

Flow pipe model for fluid circulation D2.2

Due date of deliverable: 30/09/2023
Actual submission date: 27/09/2023
Start date of project: 01/10/2022
Dissemination level: Public

Funded by the European Union. Views and opinions expressed are however those of the author(s) only and do not necessarily reflect those of the European Union or CINEA. Neither the European Union nor the granting authority can be held responsible for them.

Prepared by	Reviewed Internally by	Reviewed Externally by	Approved by
V. Leontidis (IFPEN) M. Wangen (IFE) P. Ungar (UNIFI) D. Fiaschi (UNIFI)	Mario Silva (IFE)	Ola Vestavik (RW) Domenico Liotta (UNIBA)	Mario Silva (IFE)

Technical References

Project Acronym	HOCLOOP
Project Title	A circular by design environmentally friendly geothermal energy solution based on a horizontal closed loop - HOCLOOP
Project Coordinator	IFE
Project Duration	42 months

Deliverable No.	D2.2
Dissemination level [1]	PU
Work Package	WP2
Task	2.2
Lead beneficiary	IFPEN
Contributing beneficiary(ies)	IFE, UNIFI
Prepared by /Author(s)	Vlasios Leontidis (IFPEN), Magnus Wangen (IFE), Pietro Ungar (UNIFI), D. Fiaschi (UNIFI)
Reviewed by	Ola Vestavik (RW), Domenico Liotta (UNIBA)
Approved by/Coordinator	Mario Silva (IFE)
Due date of deliverable	30/09/2023
Actual submission date	27/09/2023

[1]PU = Public
PP = Restricted to other program participants (including the Commission Services)
RE = Restricted to a group specified by the consortium (including the Commission Services)
SE = Sensitive, only for members of the consortium (including the Commission Services)

Document history

V	Date	Author(s) /Reviewer(s) (Beneficiary)	Description (examples)
0.1	07/09/2023	V. Leontidis (IFPEN), M. Wangen (IFE), P. Ungar (UNIFI), D. Fiaschi (UNIFI)	First Draft
0.2	11/09/2023	Mario Silva (IFE)	First internal revision
0.3	12/09/2023	Mario Silva (IFE)	Second draft distributed
0.4	24/09/2023	Ola Vestavik (RW) Domenico Liotta (UNIBA)	Reviewer Comments
1.0	27/09/2023	Mario Silva (IFE)	Comments Addressed, Final version
2.0	27/09/2023	Mario Silva (IFE)	Document uploaded

Disclaimer

This document is partly based on the EC's official documents and profound knowledge of guidelines and ways of working in Horizon Europe. While guidelines on administration and reporting are as much as possible the same as the official documents, adjustments have been made with logical build-up and readability in mind. However, no legal responsibility can be taken for the contents in this document. If in doubt with an issue, please consult the official documents, or ask IFE, who will ask for an official EC response if necessary.

List of Abbreviations

BHE	Borehole Heat Exchanger
BHEModel	Borehole Heat Exchanger Model
CPG	CO2 Plume Geothermal
CPA	Cubic-Plus-Association
EGS	Enhanced Geothermal System
EoS	Equation-of-States
GTW	Geo-Thermal-Well
GWellFM	Geothermal Well Flow Simulator

Table of Contents

Executive Summary Deliverable 4
1. Introduction 5
2. Methodology 6
2.1 Pipe flow equations 6
Momentum balance 6
Energy balance 7
Thermodynamic calculations 7
2.2 Numerical tools 7
GWellFM (IFPEN) 7
GTW (IFE) 8
BHEModel2.0 (UNIFI) 8
2.3 Case studies 10
Simple cases 10
Complex cases 11
3. Results 13
3.1 Simple cases 13
Case A 13
Case B 16
3.2 Complex cases 18
Case E 18
Case F 19
4. Discussions 21
4.1 Accuracy 21
4.2 Comparison of the three simulators 22
5. Conclusions 26
6. References 27

List of Figures

Figure 1. Left side: overall model scheme. Right side: schematization of the heating section representing the HOCLOOP technology (different heating sections can be considered for modelling different geothermal systems). 9
Figure 2. Graphical representation of simulated cases A (vertical well) and B (horizontal well). 10
Figure 3. Graphical representation of simulated cases E (vertical well) and F (horizontal well). 11
Figure 4. Comparison of fluid temperature along the well for case A at different times using the different simulators. 14
Figure 5. Comparison of fluid pressure (a) along the well and (b) close to the outlet (zoom) for the case A after 7 days using the different simulators. 14
Figure 6. Comparison of the temporal evolution of (a) the outlet temperature and (b) the outlet pressure of the well of case A. 15
Figure 7. Same as Figure 4 but with constant physical properties for GWellFM. 15
Figure 8. Same as Figure 5 but with constant physical properties for GWellFM. 16
Figure 9. Same as Figure 6 but with constant physical properties for GWellFM. 16
Figure 10. Comparison of fluid temperature along the well for case B at different times using the different simulators. 17
Figure 11. Comparison of fluid pressure (a) along the well and (b) close to the outlet (zoom) for the case B after 7 days using the different simulators. 17
Figure 12. Comparison of temporal evolution of (a) the outlet temperature and (b) the outlet pressure of the well of case B. 17
Figure 13. Comparison of fluid temperature along the well for case E (continuous line: annulus, dashed line: tubing) at different times using the different simulators. 18
Figure 14. Comparison of fluid pressure (a) along the well and (b) close to the outlet (zoom) for the case E after 7 days using the different simulators. 18
Figure 15. Comparison of the temporal evolution of (a) the outlet temperature, (b) the outlet pressure of the well and (c) the produced power of case E. 19
Figure 16. Comparison of fluid temperature along the well for case F at different times using the different simulators. 19
Figure 17. Comparison of fluid pressure (a) along the well and (b) close to the outlet (zoom) for the case F after 7 days using the different simulators. 20
Figure 18. Comparison of the temporal evolution of (a) the outlet temperature, (b) the outlet pressure of the well and (c) the produced power of case F. 20
Figure 19. Summary of (a) the maximum and (b) the average error (%) in the wellbore temperature estimation when comparing all tools with Ramey's solution for cases A & B and with Kabir's for cases E &F. 21
Figure 20. Summary of (a) the maximum and (b) the average error (%) when comparing the outlet temperature of the fluid between the tools for all four cases. 22
Figure 21. Summary of (a) the maximum and (b) the average error (%) when comparing the outlet pressure of the fluid between the tools for all four cases. 23
Figure 22. Summary of (a) the maximum and (b) the average error (%) when comparing the heat extracted predicted by the different calculation models in all four cases. 24
Figure 23. Comparison of (a) density, (b) viscosity, (c) thermal conductivity and (d) heat capacity for water at 30 bar and temperatures between 1 and 90°C as calculated by the three simulators. 25
Figure 24. Comparison of (a) density, (b) viscosity, (c) thermal conductivity and (d) heat capacity for water at 40°C and pressures between 1 and 40 bar as calculated by the three simulators. 25

List of Tables

Table 1. Underground, wellbore fluid and well geometry description for the simple cases. 11
Table 2. Underground, wellbore fluid and well geometry description for the complex cases. 12
Table 3. Fluid description for the calculations with the analytical solutions. 13
Table 4. Summary of the maximum and the average error (%) when comparing the outlet temperature of the fluid of all tools with Ramey's (cases A & B) or Kabir's (cases E & F) solutions. 22
Table 5. Summary of the maximum and the average error (%) when comparing the fluid outlet temperature between all tools. 23
Table 6. Summary of the maximum and the average error (%) when comparing the fluid outlet pressure between all tools. 23
Table 7. Summary of the maximum and the average error (%) when comparing the heat extracted predicted by all tools. 24

Executive Summary Deliverable

Scope of the deliverable

The objective of WP2 is to develop tools and models to predict the heat flow towards a closed-loop geothermal well and the associated temperature decrease of the surrounding rock, considering the rock properties, groundwater flow and the different layers of the walls of the well, such as casing and cement. Within WP2, Task 2.2 aims at integrating the available in-house models for the heat flow towards geothermal well from Task 2.1 in models for the heat and fluid flow in the annulus and the central pipe. The objective is to simulate different well configurations using water as pipe-fluid and test the heat transfer coefficients that control the heat flow from the well-wall interface to the fluid.

Main conclusions

Following the benchmarking of two available in-house codes, GWellFM (IFPEN) and GTW (IFE), in Task 2.1 [1], the same simulators were used to model both the fluid flow in the well, considering the hydrodynamic effects, and the heat transfer between the fluid in the well and the hosting rocks, similar to Task 2.1. In addition, a third in-house simulator, BHEModel (UNIFI) was applied. The same analytical solutions as in Task 2.1 were used to compare the results and to identify the impact considering the fluid flow. In addition, and in difference with Task 2.1, the physical properties of the fluid were pressure and temperature dependant.

The three simulators were able to reproduce the mentioned analytical solutions and they all give similar results concerning the temporal evolution of fluid's temperature. The only discrepancies between the three codes were in the early time steps. However, a stronger impact of the fluid flow and the calculation of the physical properties was shown in GWellFM.

1. Introduction

Within the context of WP2, which focuses on developing numerical tools to forecast heat transfer between the rock formation and the wellbore, Task 2.2 is dedicated to combining the heat transfer predictions (benchmarked in Task 2.1) with fluid flow models to achieve a comprehensive well model.

The models developed independently by the partners (GWellFM from IFPEN, GTW from IFE and BHEModel for UNIFI) have been compared using the methodology developed in Task 2.1. Various case studies were utilized to compare the models across a wide range of geometries. Great attention has been given to the comparison of internal heat exchange (between the annulus and the tubing) and pressure losses models.

The report has been structured as follows: The Methodology section includes a description of the various models and the equations utilized. Additionally, the selection of case studies intended for benchmarking the models is outlined. The Results section contains the comparison of the models output for the different test cases. The different models have been compared in the Discussions section, while the main findings have been summarized in the Conclusions.

2. Methodology

2.1 Pipe flow equations

Momentum balance

Similar to the heat flow described in Deliverable D2.1 [1] of the project, the fluid flow in all compartments of the well is steady-state, single-phase, 1D and axisymmetric. The pipe flow equations consisting in calculating the pressure losses due to the friction and integrated them in the pressure balance.

Generally, in pipe flows the total pressure drop per length unit [Pa/m] is the sum of the losses due to the friction and the gravity:

$$\left(\frac{dP}{dz}\right)_S = \left(\frac{dP}{dz}\right)_f + \left(\frac{dP}{dz}\right)_g \quad (1)$$

where the indices are $S = C, T$ for the casing side or the tubing space, f refers to the friction losses and g to losses due to gravity. The gravity pressure drop is:

$$\left(\frac{dP}{dz}\right)_g = \rho\, g \sin\theta \quad (2)$$

with g [m^2/s] the acceleration of gravity, ρ [kg/m^3] the fluid density and ϑ [°] the inclination of the well (0° if the pipe is horizontal, 90° if the pipe is vertical).

For single-phase flow, the pressure losses due to friction can be calculated by the well-known Darcy–Weisbach equation:

$$\left(\frac{dP}{dz}\right)_f = \frac{f\rho u^2}{2D_h} \quad (3)$$

where u [m/s] is the velocity of the fluid, D_h [m] is the hydraulic diameter and f is the Darcy friction factor. For laminar flow it is a consequence of Poiseuille's law:

$$f = \frac{64}{Re}, Re < 1000 \quad (4)$$

whereas for higher Reynolds numbers it can be calculated from the Colebrook-White equation [2]:

$$\frac{1}{\sqrt{f}} = -2.0 log\left(\frac{\varepsilon}{3.7D_h} + \frac{2.51}{Re\sqrt{f}}\right) \quad (5)$$

where ε [m] is the roughness of the pipe wall and the Reynold number is:

$$Re = \frac{D_h u \rho}{\mu} \quad (6)$$

with μ [Pa.s] fluid's viscosity.

A mathematically equivalent expansion of the Colebrook equation is:

$$\frac{1}{\sqrt{f}} = 1.1364 - 2.0log\left(\frac{\varepsilon}{D_h} + \frac{9.287}{Re\sqrt{f}}\right) \quad (7)$$

Several, approximations of the Colebrook equation exist, such as the standard Churchill formulation, which is valid both for laminar and turbulent flows:

$$f = 8\left[\left(\frac{8}{Re}\right)^{12} + \left(\frac{1}{\Theta_1 + \Theta_2}\right)^{\frac{3}{2}}\right]^{\frac{1}{12}} \quad (8)$$

$$\Theta_1 = \left[2.457\ \ln\left(\frac{1}{\left(\frac{7}{Re}\right)^{\frac{9}{10}} + 0.27\frac{\varepsilon}{D_h}}\right)\right]^{16} \quad (9)$$

$$\Theta_2 = \left(\frac{37530}{Re}\right)^{16} \quad (10)$$

Energy balance

When the fluid flow in the well is considered, the energy balance must be modified, in comparison with the one applied in the benchmarking of the tools [1], to consider the heat losses due to friction:

$$\frac{d}{dz}[\dot{m}\rho(H - zg\sin\theta)] = -Q \quad (11)$$

where *H* [J/kg] is the specific enthalpy of the fluid and *Q* [W/m] are the heat losses.

Thermodynamic calculations

It should be also noted that, differently from the approach of Deliverable D2.1, the physical properties of the fluid were pressure and temperature dependant. Either lookup tables were used, or thermodynamic tools were integrated in the available codes to perform calculations in thermodynamic equilibrium with specific Equation-of-States (EoS).

2.2 Numerical tools

GWellFM (IFPEN)

GWellFM (Geothermal Well Flow Model) solves successively and iteratively the steady-state momentum, Eq. (1), and the enthalpy, Eq. (11), balances at every cell along an axial mesh in the well. The heat flow (the term *Q* in the energy equation) from the hosting formation to the well is numerically computed by solving the 2D transient Fourier heat conduction equation, as previously described in Deliverable D2.1 [1]. The differences with the simulations performed in Task 2.1 and detailed in the corresponding Deliverable are:

- Friction losses both in the momentum and the enthalpy balances are considered.
- The friction factor is calculated with Eq. (5).
- The transport properties (density, viscosity, heat capacity and thermal conductivity) of the fluid (water) are temperature and pressure dependent and the integrated thermodynamic tool is used to perform calculations in thermodynamic equilibrium using the CPA (Cubic-Plus-Association) EoS.

The energy equation, Eq. (11), was further expanded to consider the temperature instead of the enthalpy for comparison reasons with the analytical solutions and the other codes [1]. For performing thermodynamic calculations, an internal tool (Carnot) has been integrated in GWellFM.

GTW (IFE)

GTW (GeoThermal Well) solves two equations iteratively in the case of an incompressible fluid. Firstly, a temperature equation for the rock and the well [1], and secondly, a pressure, Eq. (1), and a temperature, Eq. (11), equation for the pipe flow in the well. The first equation accounts for the transient cooling of the well, when the properties of the fluid are given, and the second equation solves for pressure and temperature in the well when the heat flow through the pipe walls is given. The basis for the first equation is energy conservation of the combined system of the pipe and rock, and the section equation is mass, momentum and energy conservation in the pipe. Furthermore, the fluid flow in the pipe is assumed to be in a stationary state. The energy conservation of the combined system of the rock and pipes are solved with a fully implicit upstream energy conservative finite volume method. Therefore, the time stepping is unconditionally stable. The second equation, the stationary state of the pipe is found by integration downstream from the pipe inlet to the outlet.

These two equations are solved by an iteration loop. The temperature equation for the well and the rock is solved first using the fluid properties from the previous time step or the previous iteration. This step provides the heat flow through the walls of the pipe. The next step solves for the temperature and the pressure in the pipe given the external heat flow. This second step provides fluid properties, which are used in the first step of the next iteration. More than two iterations are rarely needed per time step.

Fluid properties such as density, thermal expansibility, compressibility, viscosity and enthalpy are taken from tables. The simulations in this report are done with tables for H_2O. The tables are equidistant in the steps of pressure and temperature which makes look-up and interpolation a fast operation. The momentum equation accounts for friction, as given by Eq. (7).

BHEModel2.0 (UNIFI)

UNIFI model has been developed extending an existing model used for theoretical analysis on geothermal systems [3]. The original model was conceived to represent a variety of geothermal systems (EGS, CPG, BHE, etc.) simply by replacing the heating section, as depicted in Figure 1. The model has been modified to comply with the specific HOCLOOP geometry.

The evolution of pressure and enthalpy are given by Eqs. (1) and (11). The pressure losses have been evaluated using the standard Churchill formulation with Eqs. (8)-(10). The heat transfer in the pipe is evaluated considering the thermal resistances, R_ϑ [m K/W], of the different parts:

$$Q = R_{\theta,int}\,\Delta T_{int} + R_{\theta,ext}\,\Delta T_{ext} \tag{12}$$

where only the annulus has the internal contribution. The thermal resistances are evaluated as follows:

$$R_{\theta,int} = \frac{1}{\pi D_{ti} h_{ti}} + \frac{1}{\pi D_{to} h_{to}} + \frac{\ln\left(\frac{D_{to}}{D_{ti}}\right)}{2\pi k_t} \tag{13}$$

$$R_{\theta,ext} = \frac{1}{\pi D_{ci} h_{ci}} + \frac{\ln\left(\frac{D_{co}}{D_{ci}}\right)}{2\pi k_c} + R_{\theta,e} \tag{14}$$

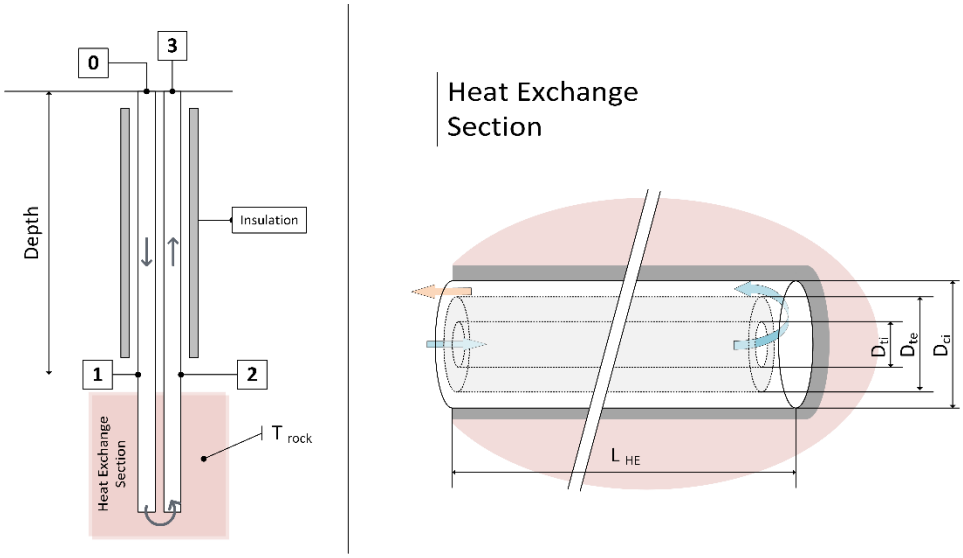

Figure 1. Left side: overall model scheme. Right side: schematization of the heating section representing the HOCLOOP technology (different heating sections can be considered for modelling different geothermal systems).

with *k* [W/m/K] the thermal conductivity of the solid material (*t*: tube, *c*: casing), *D* [m] the corresponding diameter (*i*: internal, *o*: external) and *h* [W/m^2/K] the forced convective heat transfer coefficient of the fluid calculated considering the turbulent Nusselt number as follows:

$$h = \frac{Nu\, k_{fluid}}{D_h} \tag{15}$$

where D_h is the hydraulic diameter, k_{fluid} is the fluid heat conductivity and:

$$Nu = 0.023 Re^{0.8} Pr^{0.4} \tag{16}$$

The heat transfer in the rocks has been evaluated following the same approach of Zang et al. [4] based on the approximate solution of the heat transfer problem provided by Carslaw & Jaeger [5]:

$$R_{\theta,e} = \pi k_e\, f(t_d) \tag{17}$$

with the time function:

$$f(t_d) = \begin{cases} \frac{1}{2} + (\pi t_d)^{-\frac{1}{2}} - \frac{1}{4}\left(\frac{t_d}{\pi}\right)^{\frac{1}{2}} + \frac{1}{8} t_d, & t_d < 2.8 \\ \frac{2}{\ln(4t_d) - 2\gamma} - \frac{2\gamma}{(\ln(4t_d) - 2\gamma)^2}, & t_d \geq 2.8 \end{cases} \tag{18}$$

In the above equation $t_d = \alpha_e t / D_{co}^2$ is a dimensionless time, $\alpha_e = k_e / \rho_e C_{pe}$ is the thermal diffusivity of the rocks and γ is Euler's constant. Equation (17) can be directly used to retrieve thermal resistance in case of stationary flow. On the other hand, if a significant fluctuation of the flow rate in the well is expected, a convolution approach can be used to estimate the evolution over time of the temperatures around the well [5].

The system has been integrated through the well using a fifth order Runge-Kutta solver [6] as implemented in the python SciPy library [7]. The fluid properties are retrieved using REFPROP [8] which is a commercial software developed by NIST that implements a modified version of the Benedict-Webb-Rubin Equation-of-State. REFPROP is known for its accuracy, especially for pure fluids composed of simple molecules so that it is sometimes used for benchmarking of other software [9]. The system has been integrated using pressure and density (instead of pressure and enthalpy) due to some stability issue with REFPROP in the lower temperature water region. The density derivative has been calculated as follows:

$$\frac{d\rho}{dz} = \left[\frac{\partial\rho}{\partial P}_T + \frac{\frac{\partial\rho}{\partial T}_p}{\frac{\partial h}{\partial T}_p}\left(\frac{dH}{dP} - \frac{\partial H}{\partial P}_T\right)\right]\frac{dP}{dz} \tag{19}$$

The total derivatives ($\frac{dH}{dP}$ and $\frac{dP}{dz}$) are evaluated starting from Eqs. (1) and (11), while the partial derivatives can be directly evaluated using REFPROP.

2.3 Case studies

Two simple and two complex cases from Deliverable D2.1 [1] were selected to be used here. The three available simulators are applied for the same conditions and the results will be later compared. For the complex cases, some modifications of the well geometry were necessary to avoid issues resulting of high pressure losses.

Simple cases

Cases A and B are, respectively, a vertical and a horizontal complete cased wells (Figure 2). The wells are considered to open to the reservoir (serve as injectors). Table 1 summarizes the configurations of the two cases.

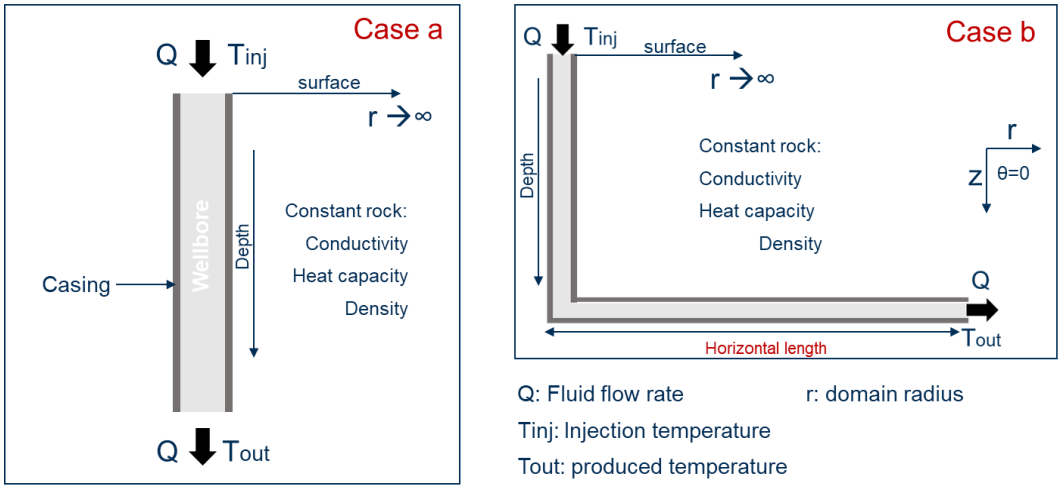

Figure 2. Graphical representation of simulated cases A (vertical well) and B (horizontal well).

Table 1. Underground, wellbore fluid and well geometry description for the simple cases.

Case	A	B
Rock thermal conductivity [W/m/K]	2.423	2.423
Bulk rock density [kg/m^3]	2600	2600
Rock specific heat capacity [J/kg/K]	902.67	902.67
Surface temperature [°C]	21.111	11
Thermal gradient [°C/m]	0.01513	0.0325
Type of fluid	Water	Water
Injection temperature [°C]	14.72	45.00
Injection pressure [bar]	10	10
Fluid flow rate [kg/s]	8.8	8.8
Completion	Totally cased	Totally cased
Type of directional well	Vertical	Horizontal
Vertical depth [m]	1828.8	3000
Horizontal section length [m]	--	3500
Total depth [m]	1828.8	6500
Casing internal diameter [m]	0.1617	0.1617
Casing external diameter [m]	0.1778	0.1778
Casing thermal conductivity [W/m/K]	43.268	43.268

Complex cases

Case E and F are a vertical and a horizontal pipe-in-pipe fully cased wells (Figure 3) closed at the end. The fluid is injected in the annulus side and recovered at the surface from the central tubing. Table 2 summarizes the configurations of the two cases.

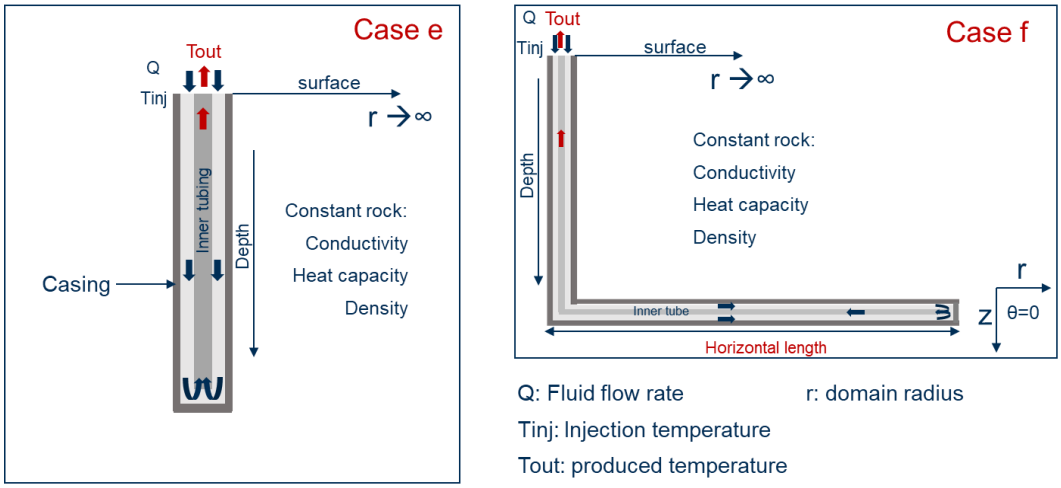

Figure 3. Graphical representation of simulated cases E (vertical well) and F (horizontal well).

Table 2. Underground, wellbore fluid and well geometry description for the complex cases.

Case	E	F
Rock thermal conductivity [W/m/K]	2.423	2.423
Bulk rock density [kg/m^3]	2600	2600
Rock specific heat capacity [J/kg/K]	902.67	902.67
Surface temperature [°C]	21.111	11
Thermal gradient [°C/m]	0.01513	0.0325
Type of fluid	Water	Water
Injection temperature [°C]	14.72	45.00
Injection pressure [bar]	10	40
Fluid flow rate [kg/s]	8.8	8.8
Completion	Totally cased	Totally cased
Type of directional well	Vertical	Horizontal
Vertical depth [m]	1828.8	3000
Horizontal section length [m]	--	3500
Total depth [m]	1828.8	6500
Casing internal diameter [m]	0.2917	0.1617
Casing external diameter [m]	0.3078	0.1778
Casing thermal conductivity [W/m/K]	43.268	43.268
Inner tubing internal diameter [m]	0.08	0.1
Inner tubing external diameter [m]	0.13	0.13
Inner tubing thermal conductivity [W/m/K]	0.1	0.1

3. Results

The tree simulators, GTW (IFE), GWellFM (IFPEN) and BHEModel (UNIFI), were evaluated against analytical solutions. GTW and GWellFM model the heat flow in the rock by numerical approaches while BHEModel integrates an analytical approach. The computed temperature profiles along the well were compared with the same analytical solutions applied in Task 2.1, using constant physical properties for the fluid. For the analytical solutions, the physical properties of the fluid were always constant (Table 3).

Table 3. Fluid description for the calculations with the analytical solutions.

Case	A, B, E, F
Type of fluid	Water
Compressibility [bar^{-1}]	0
Heat capacity [J/kg/K]	4196
Density [kg/m^3]	998.554
Thermal conductivity [W/m/K]	0.5867
Viscosity [Pa.s]	0.0011

3.1 Simple cases

Case A

This case corresponds to the injection of water with a temperature lower than the rock temperature in a vertical well. All simulators predicted a continuous increase of the temperature as the water flows down in the well. These forecasts follow Ramey's analytical solutions [10] as shown in Figure 4 for different simulation times and in Figure 6a for the outlet temperature. When compared to the analytical solution, GTW and BHEModel showed better agreement rather than GWellFM. The solutions of GTW and BHEModel are almost overlapping. In comparison with the results of Task 2.1 [1], both GTW and GWellFM predicted slightly higher fluid temperature, which results from the consideration of the friction and the fact that the physical properties of the fluid were not constant.

Ramey's analytical solution is generally known not to be very accurate at early time steps and to overestimate fluid's temperature (for the specific study case). The three simulators also gave different results at early times (below 3 days), but later all of them converged to almost the same value (Figure 6a).

All simulators predicted similar pressure evolution with the GWellFM giving continuously higher pressures. The results for all times steps were similar as in Figure 5. Figure 6b gives the evolution of the outlet pressure over time. Again, the predictions of GWT and BHEModel were closer than those of GWellFM.

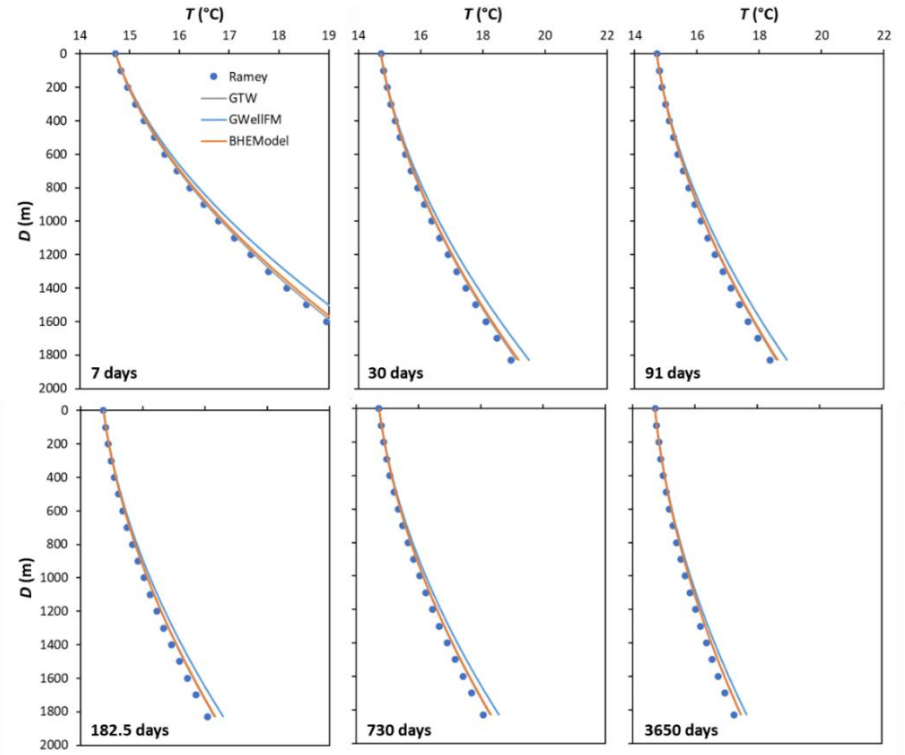

Figure 4. Comparison of fluid temperature along the well for case A at different times using the different simulators.

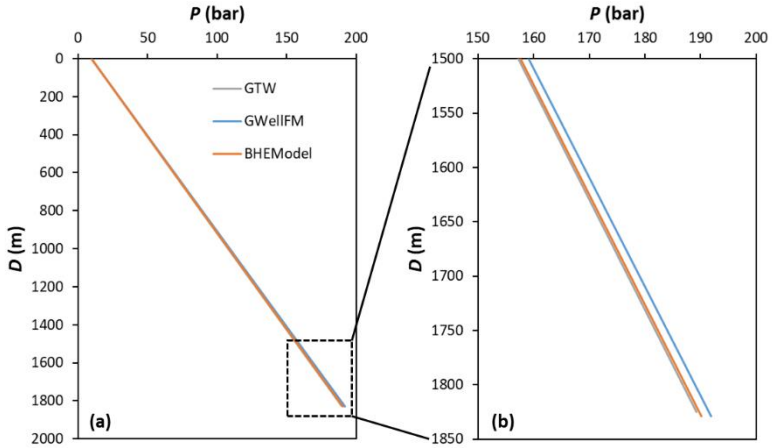

Figure 5. Comparison of fluid pressure (a) along the well and (b) close to the outlet (zoom) for the case A after 7 days using the different simulators.

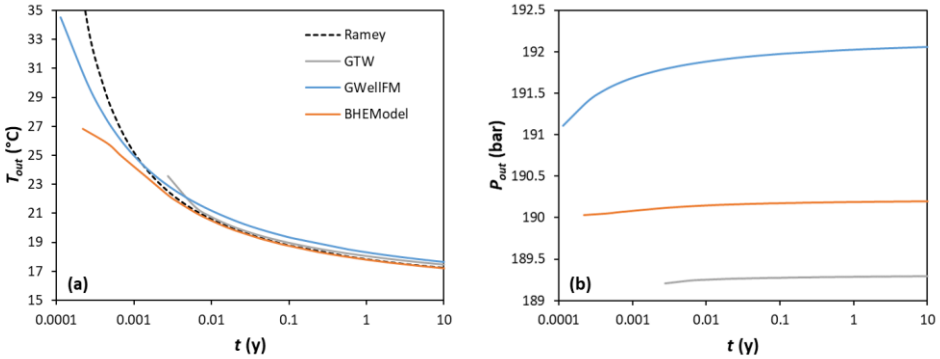

Figure 6. Comparison of the temporal evolution of (a) the outlet temperature and (b) the outlet pressure of the well of case A.

To identify if these differences between GWellFM and the two other simulators were due to the physical properties' calculation, the same case was run with GWellFM but imposing constant physical properties (denoted as case A2). The results are presented in Figure 7, Figure 8 and Figure 9. In this case, the results of GWellFM matched the analytical solution and were closer to the other two codes. This indicates that the contribution of friction in the energy balance is marginal, as expected, and doesn't affect the results. On the other hand, the physical properties and their calculations have quite a strong impact.

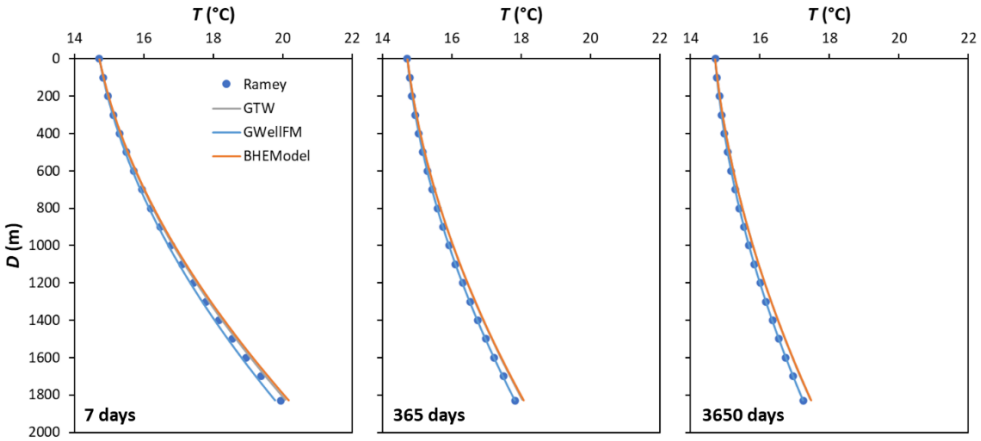

Figure 7. Same as Figure 4 but with constant physical properties for GWellFM.

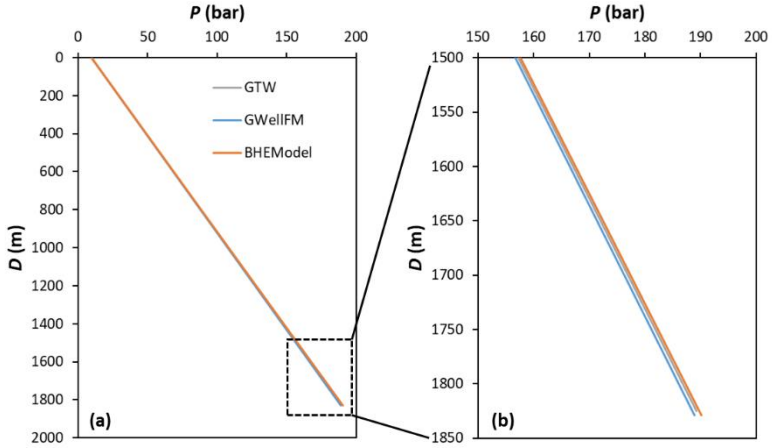

Figure 8. Same as Figure 5 but with constant physical properties for GWellFM.

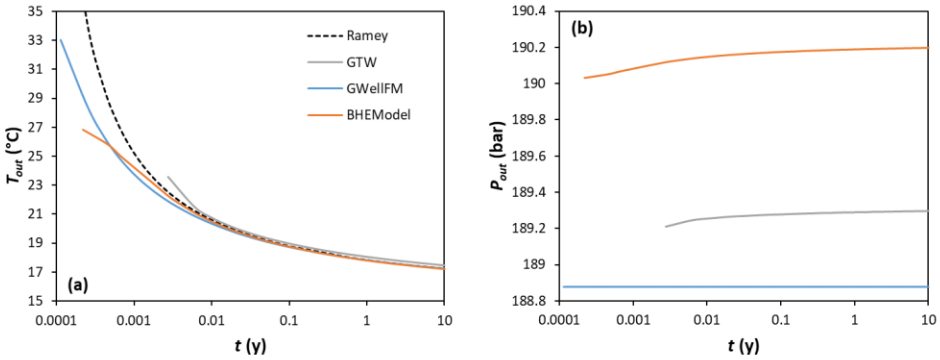

Figure 9. Same as Figure 6 but with constant physical properties for GWellFM.

Case B

The heat transfer in a horizontal injector well without a returning pipe was evaluated in this case. Results of fluid's temperature and pressure evolution along the well are shown in Figure 10 and Figure 11 respectively, while in Figure 12 the time evolution of the outlet temperature and pressure are presented. The presence of the horizontal section with initial constant temperature makes the temperature profile to changes in slope. As previously, the simulations were able to follow the modified Ramey's solution [1], including the decrease in temperature at shallow depths due to heat leakage from the well to the surrounding rock. For this case, all codes give similar results with GWellFM estimating slightly higher temperature and pressure. As before for case A, when compared the results with Task 2.1, GWT and GWellFM predicted slightly higher temperatures due to the different parameters of the models.

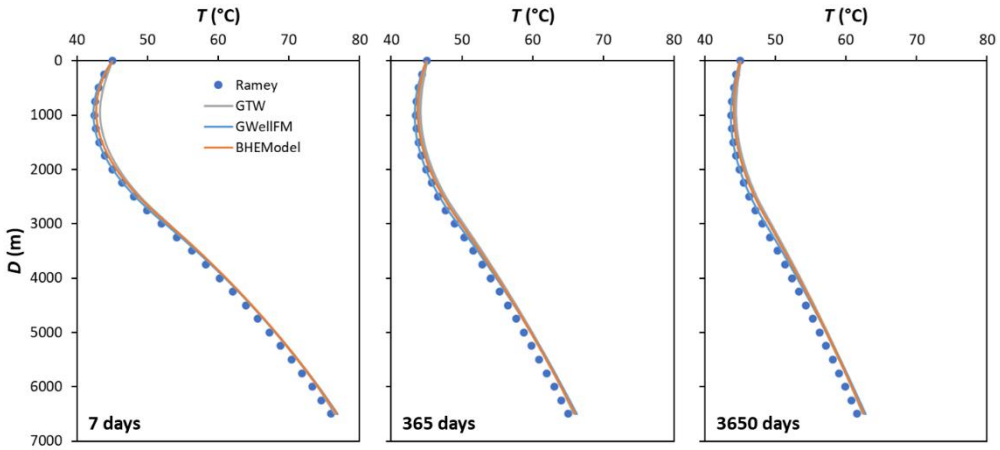

Figure 10. Comparison of fluid temperature along the well for case B at different times using the different simulators.

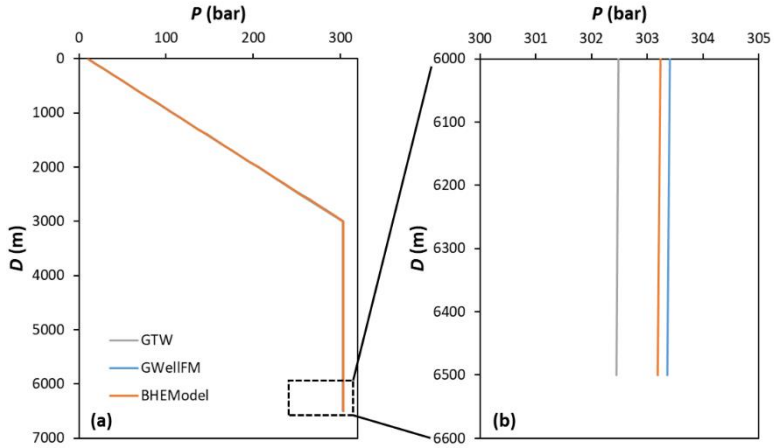

Figure 11. Comparison of fluid pressure (a) along the well and (b) close to the outlet (zoom) for the case B after 7 days using the different simulators.

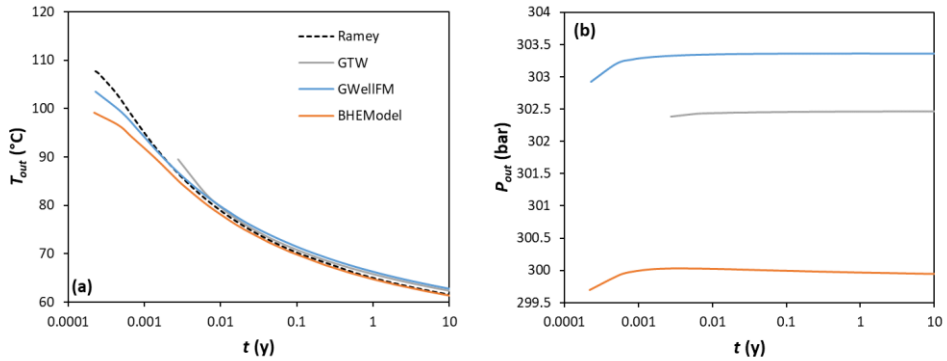

Figure 12. Comparison of temporal evolution of (a) the outlet temperature and (b) the outlet pressure of the well of case B.

3.2 Complex cases

For estimating the maximum theoretical heat extraction, Q [W], the below equation is introduced for the coaxial cases E and F:

$$Q = \dot{m}(H_{out} - H_{in}) = \dot{m}C_{pf}\left(T_{f,prod} - T_{f,inj}\right) \quad (20)$$

Case E

The heat extraction in a vertical well with a coaxial returning pipe was tested in this case. The capacity of the simulators to model the heat losses in the returning pipe were compared with Kabir's analytical solution [11]. The exact form of the equation can be also found in Deliverable D2.1 of the project. Figure 13 shows the temperature profile in the annulus (injection: continuous line) and in the return coaxial tubing (production: dashed line) and Figure 14 the corresponding pressure evolution. As above, GWellFM predicted slightly higher temperature and pressure (Figure 15a, b), and lower heat extraction (Figure 15c).

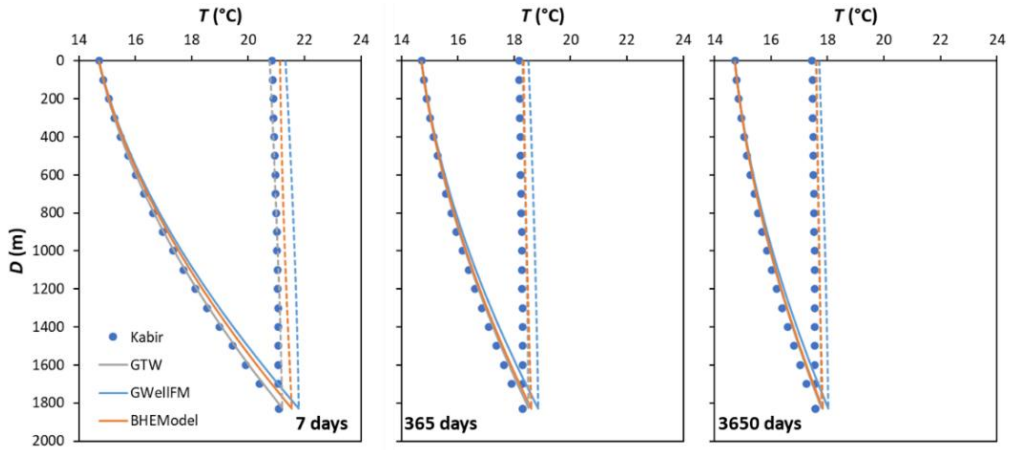

Figure 13. Comparison of fluid temperature along the well for case E (continuous line: annulus, dashed line: tubing) at different times using the different simulators.

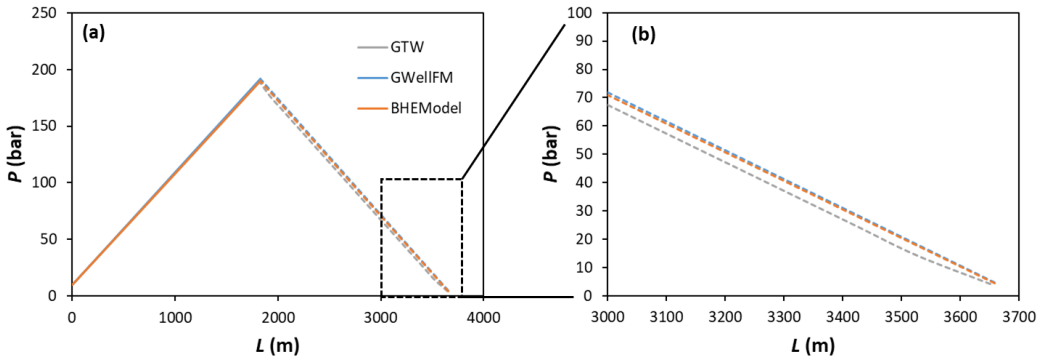

Figure 14. Comparison of fluid pressure (a) along the well and (b) close to the outlet (zoom) for the case E after 7 days using the different simulators.

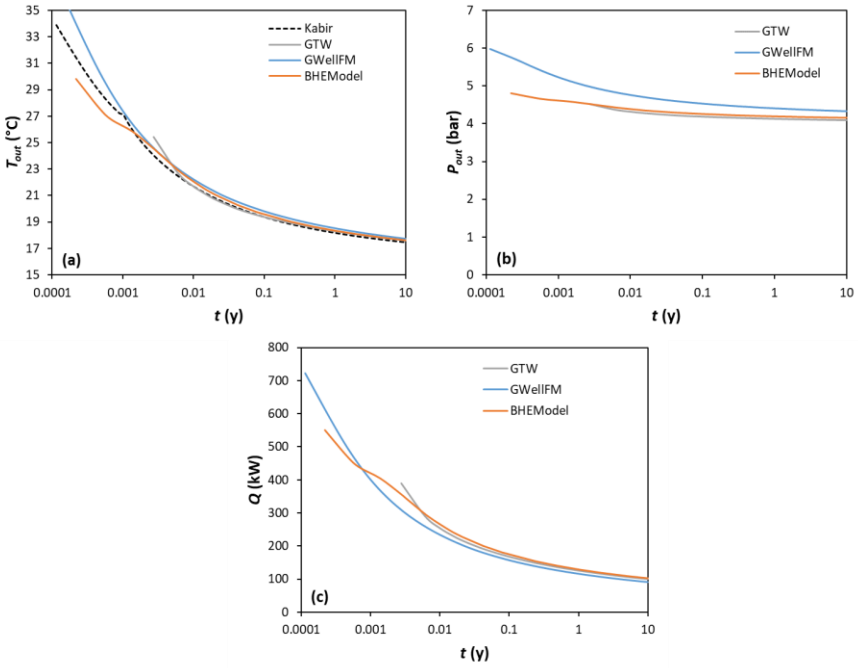

Figure 15. Comparison of the temporal evolution of (a) the outlet temperature, (b) the outlet pressure of the well and (c) the produced power of case E.

Case F

In this case, the ability of the simulators to model the coaxial closed-loop system in a horizontal well was evaluated (the HOCLOOP concept). The results of the temperature prediction were compared with Kabir's analytical solution [12]. The results are shown in Figure 16, Figure 17 and Figure 18. The findings are similar with the previous cases with GWellFM giving slightly higher fluid's temperature and pressure, and GTW and GWellFM predicting higher temperatures when compared with the corresponding values of Task 2.1. However, BHEModel's divergence was higher for this case in comparison with the previous cases or the other simulators when comes to the outlet temperature.

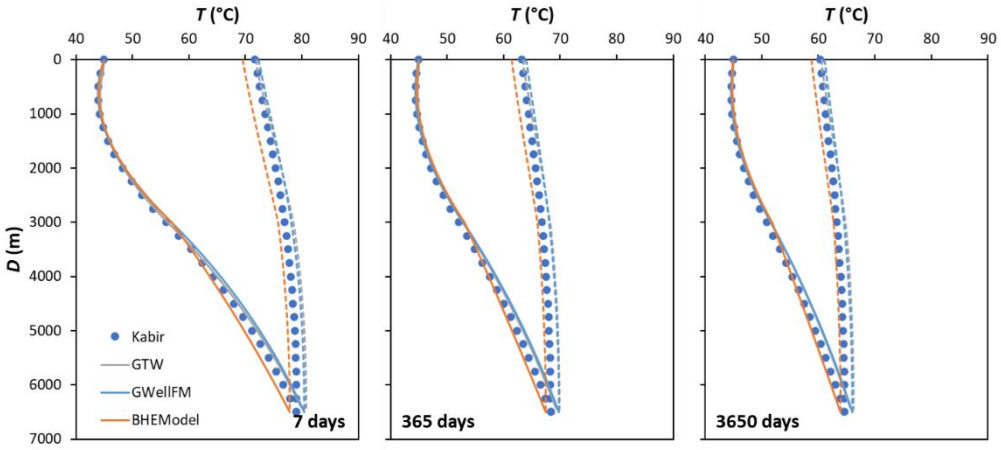

Figure 16. Comparison of fluid temperature along the well for case F at different times using the different simulators.

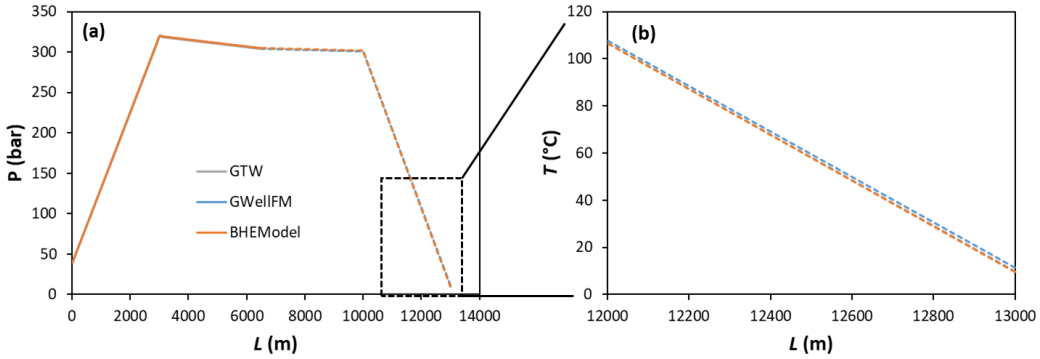

Figure 17. Comparison of fluid pressure (a) along the well and (b) close to the outlet (zoom) for the case F after 7 days using the different simulators.

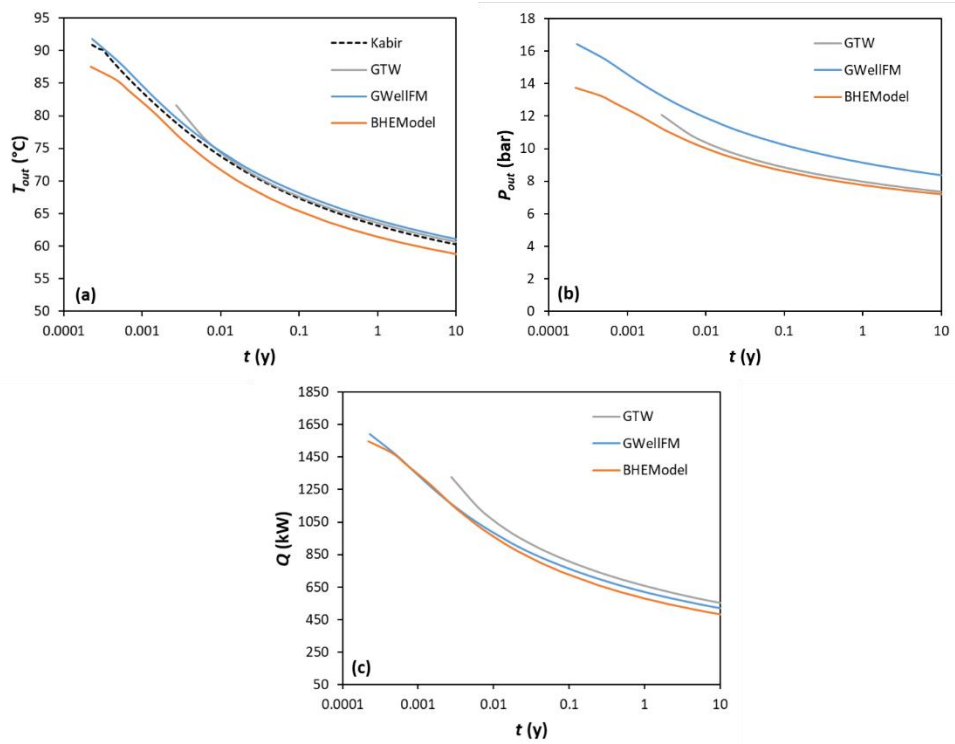

Figure 18. Comparison of the temporal evolution of (a) the outlet temperature, (b) the outlet pressure of the well and (c) the produced power of case F.

4. Discussions

To compare the results of the different models, the relative error δ , between the temperature calculated with a reference method, i.e., Ramey's solution, and the temperature predicted by the simulators, T_{pred}, is introduced:

$$\delta = \frac{T_{ref} - T_{pred}}{T_{ref}} 100 \quad (21)$$

The results of the different simulators are compared against Ramey solutions at specific times and at different depths in the well. For the coaxial wells, all simulators calculate the temperature along the annulus but also in the central tubing, whereas Ramey solution calculates the temperature evolution in the annulus only.

To compare the three simulators, the relative error, δ, is defined as:

$$\delta = \frac{\Phi_1 - \Phi_2}{\Phi_1} 100 \quad (22)$$

where Φ is either the temperature or the pressure, and the subscripts 1 and 2 correspond to two simulators.

4.1 Accuracy

As in Deliverable 2.1 [1], the results of all codes were compared with the available analytical solutions. Figure 19 and Table 4 show the maximum and the average errors based on all computed points along the well. Ramey's analytical solution was used as a benchmark for cases A and B, while Kabir's analytical solutions were used for cases E and F. All the three codes show a good agreement when compared to the analytical solutions, with an average error below 3%. The case A2 corresponds to the GWellFM with constant physical properties, which gave the minimum average error (less than 0.5%).

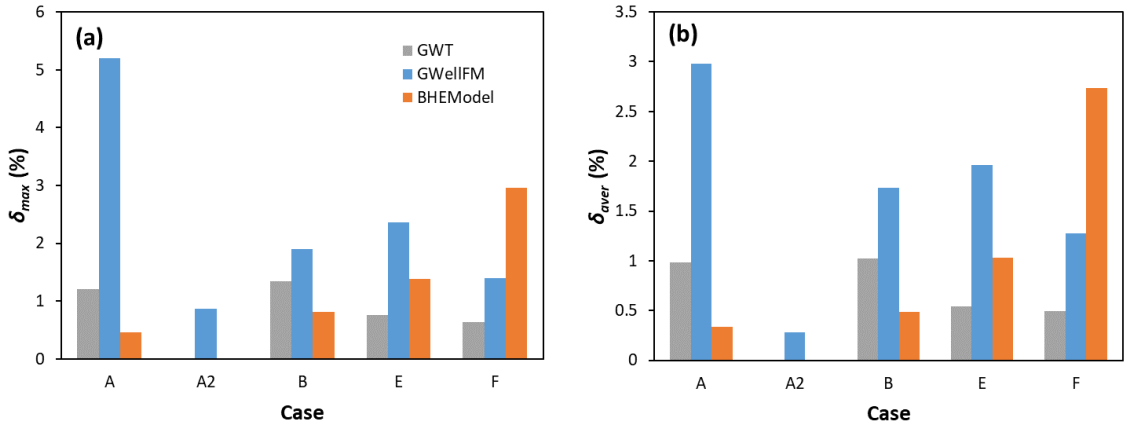

Figure 19. Summary of (a) the maximum and (b) the average error (%) in the wellbore temperature estimation when comparing all tools with Ramey's solution for cases A & B and with Kabir's for cases E &F.

When compared to the analytical solutions, GTW and BHEModel seems to be more accurate. However, it should be noted that BHEModel applies a similar analytical solution for calculating the heat transfer between the well and fluid, and that GTW uses tables for finding fluid's properties. As previously shown, with GWellFM and constant properties the numerical results match the analytical ones.

Table 4. Summary of the maximum and the average error (%) when comparing the outlet temperature of the fluid of all tools with Ramey's (cases A & B) or Kabir's (cases E & F) solutions.

Case	GWT (IFE)		GWellFM (IFPEN)		BHEModel (UNIFI)	
	Average [%]	Maximum [%]	Average [%]	Maximum [%]	Average [%]	Maximum [%]
A	0.984	1.213	2.979	5.199	0.338	0.463
A2			0.280	0.870		
B	1.025	1.343	1.734	1.902	0.489	0.819
E	0.541	0.757	1.966	2.361	1.029	1.377
F	0.494	0.639	1.276	1.393	2.739	2.958

4.2 Comparison of the three simulators

The maximum and average differences when the simulators are compared each other, are shown in Figure 20 and Table 5 for the outlet temperature, Figure 21 and Table 6 for the outlet pressure, and Figure 22 and Table 7 for the heat extraction.

The comparisons between GWT and BHEModel showed the lower error for all cases except case F, for which BHEModel had the higher divergence when comparing to the analytical solution of Kabir. On the other hand, GWellFM with constant physical properties (case A2) had the minimum error when compared with the other two simulators.

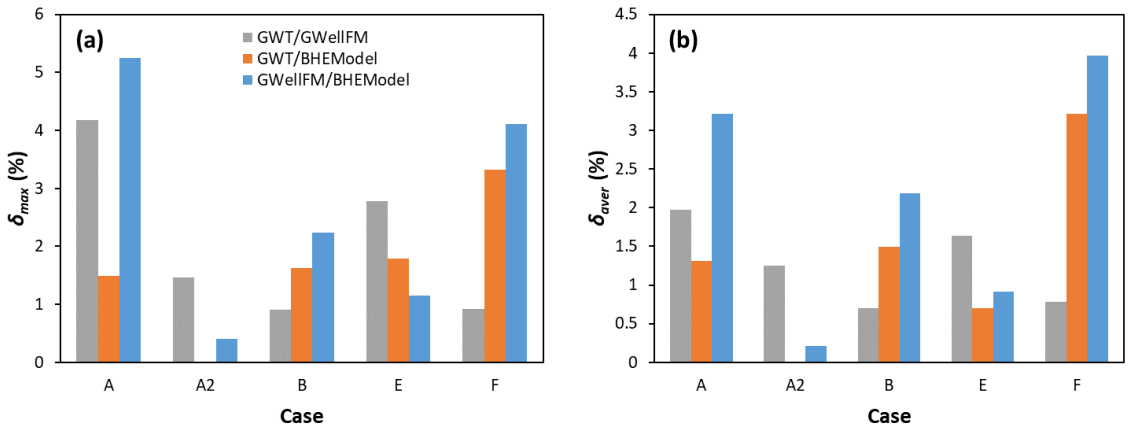

Figure 20. Summary of (a) the maximum and (b) the average error (%) when comparing the outlet temperature of the fluid between the tools for all four cases.

Table 5. Summary of the maximum and the average error (%) when comparing the fluid outlet temperature between all tools.

Case	GWT/GWellFM		GWellFM/BHEModel		GWT/BHEModel	
	Average [%]	Maximum [%]	Average [%]	Maximum [%]	Average [%]	Maximum [%]
A	1.976	4.176	3.215	5.246	1.309	1.495
A2	1.252	1.457	0.207	0.411		
B	0.702	0.905	2.185	2.238	1.498	1.631
E	1.632	2.779	0.919	1.149	0.697	1.791
F	0.778	0.918	3.964	4.105	3.217	3.316

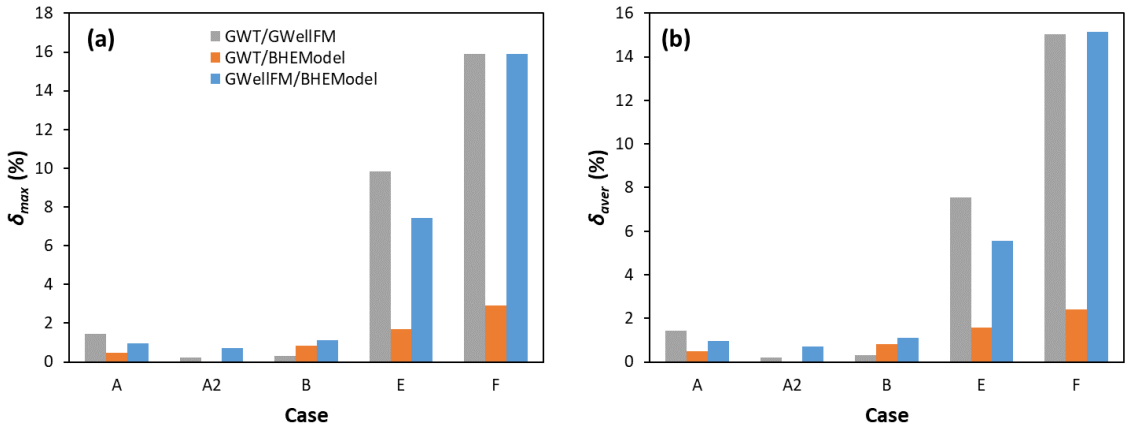

Figure 21. Summary of (a) the maximum and (b) the average error (%) when comparing the outlet pressure of the fluid between the tools for all four cases.

Table 6. Summary of the maximum and the average error (%) when comparing the fluid outlet pressure between all tools.

Case	GWT/GWellFM		GWellFM/BHEModel		GWT/BHEModel	
	Average [%]	Maximum [%]	Average [%]	Maximum [%]	Average [%]	Maximum [%]
A	1.434	1.459	0.946	0.969	0.475	0.476
A2	0.215	0.221	0.691	0.699		
B	0.297	0.299	1.115	1.125	0.821	0.834
E	7.559	9.831	5.560	7.448	1.565	1.688
F	15.049	15.880	15.163	15.902	2.400	2.928

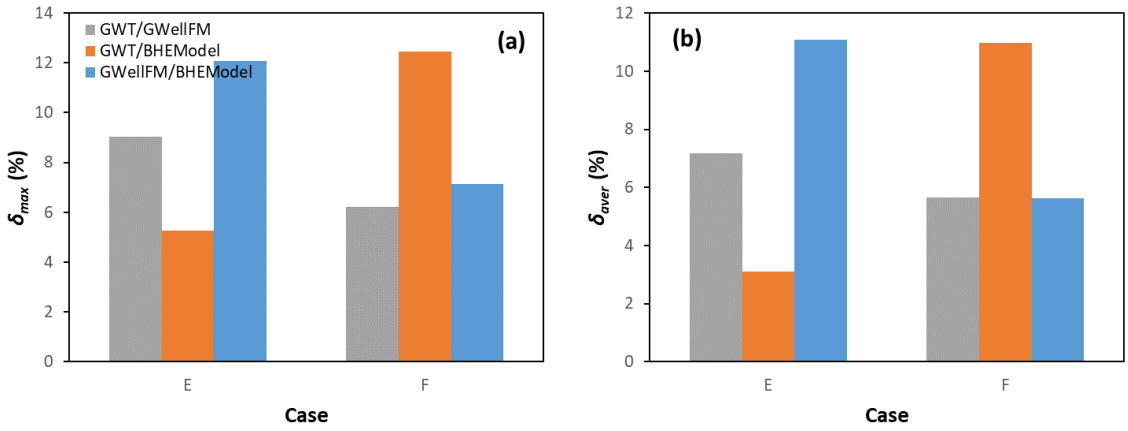

Figure 22. Summary of (a) the maximum and (b) the average error (%) when comparing the heat extracted predicted by the different calculation models in all four cases.

Table 7. Summary of the maximum and the average error (%) when comparing the heat extracted predicted by all tools.

Case	GWT/GWellFM		GWellFM/BHEModel		GWT/BHEModel	
	Average [%]	Maximum [%]	Average [%]	Maximum [%]	Average [%]	Maximum [%]
E	7.172	9.037	11.082	12.073	3.114	5.259
F	5.660	6.205	5.625	7.134	10.968	12.449

The physical properties (density, ρ, viscosity, μ, thermal conductivity, k, and heat capacity, Cp) were calculated with each tool in the range of 1-40 bar and 1-90°C. In the plots of Figure 23 the results of the evolution of the properties with temperature at 30 bar are shown, and in Figure 24 the evolution of the properties with pressure at 40°C. The results for all other pressures or temperatures were similar. The table method in GTW and the tool RERPROP in BHEModel are giving overlapping curves, whereas Carnot in GWellFM gives different density and heat capacity. With GWellFM's tool, the changes in the density and the heat capacity with the temperature are stronger and the values different from those used in the calculations with the analytical solutions (Table 3). This observation explains why GWellFM differs from the other tools and the analytical results.

For cases E and F, the heat extraction has the maximum error, higher than the corresponding temperature error (Figure 22, Table 7), even between GWT and BHEModel. According to Eq. (20), the value depends either on the enthalpy estimation with thermodynamic tools which apparently adds additional errors. However, the outlet temperature is the most important parameter and not the power.

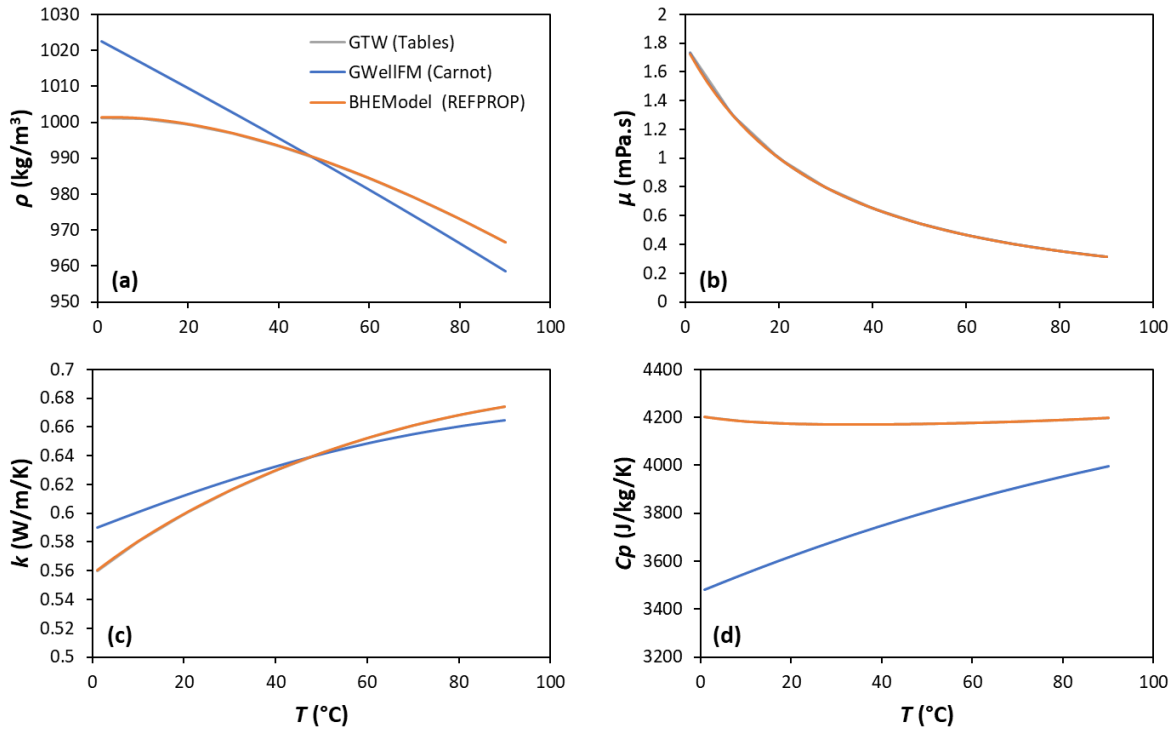

Figure 23. Comparison of (a) density, (b) viscosity, (c) thermal conductivity and (d) heat capacity for water at 30 bar and temperatures between 1 and 90°C as calculated by the three simulators.

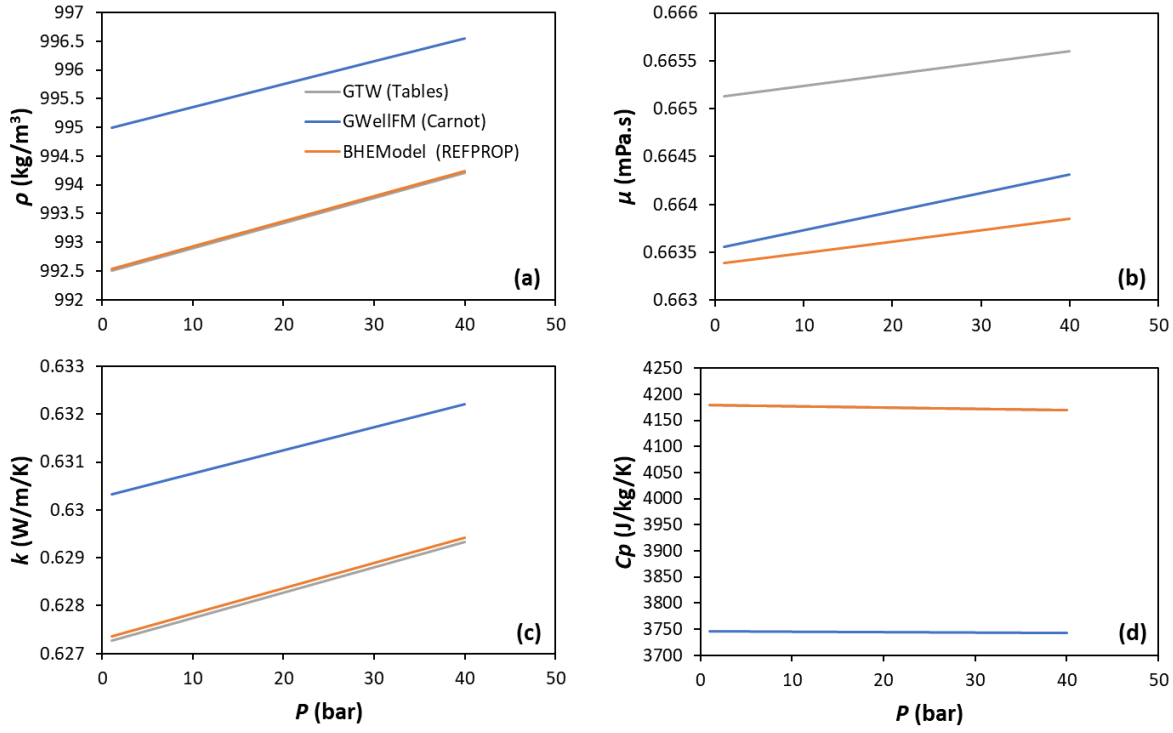

Figure 24. Comparison of (a) density, (b) viscosity, (c) thermal conductivity and (d) heat capacity for water at 40°C and pressures between 1 and 40 bar as calculated by the three simulators.

5. Conclusions

Three different simulators were compared on the same well heat exchange cases: GWellFM (IFPEN), GTW (IFE) and BHEModel (UNIFI). All cases were completed by the three simulators and compared with the corresponding analytical solutions showing the ability of their capability in predicting correctly the temperature evolution of the fluid in the well.

All the simulators can model conductive heat exchange in vertical and horizontal wells, including closed-loop well completions like the HOCLOOP concept. They can also account for vertical heterogeneous rocks, changing temperature gradients and wells with multiple walls (i.e., casing, cement, insulation) and complex geometries (i.e., changing diameter along the well).

For cases that involved injection of a fluid without recirculation of the fluid (cases A and B), the simulators presented an average error between 0.3 and 3% when compared to Ramey's analytical solution for the temperature. The average error of the simulators when modelling closed-loop cases, such the HOCLOOP concept (case E and F) was equal or lower than 2.8%, when compared to the Kabir's analytical solutions. In all cases, the highest difference either between the tools and the analytical solutions or between the tools each other was observed at the early time steps. However, the temperature was always converging at the same values.

The simulators can also simulate the evolution of the fluid pressure, considering the pressure losses due to friction and gravity. When the three codes were compared with each other, GWellFM showed the larger difference, with GWT and BHEModel giving similar results with an average error between 0.3 and 2.4%.

The discrepancy between GWellFM and the other two codes is attributed mainly to the difference in the physical properties. When GWellFM was run applying constant physical properties (case A2) the errors in the temperature and the pressure were decreased in comparison to the analytical solution or the two other simulators. A comparison of all physical properties revealed that the density and the heat capacity in GWellFM are different from the corresponding values of GWT and BHEModel.

Computing the heat extraction as the difference in the enthalpy between outlet and inlet for cases E and F, resulted in the highest error when all three codes were compared. The errors were higher from the corresponding temperature difference. But again, the errors are coming mainly from the thermodynamic tools available in each code and the calculation of the enthalpy.

6. References

[1] E. Acevedo, V. Leontidis, M. Wangen and V. Harcouët-Menou, “Benchmark cases D2.1,” HOCLOOP Project 101083558, 2023.

[2] W. Stewart, R. Bird and E. Lightfoot, Transport Phenomena, New York: J. Wiley, 2001.

[3] P. Ungar, D. Fiaschi, G. Manfrida et L. Talluri, «Thermodynamic Assessment of Geothermal High-Temperature Heat Pumps for Industrial Steam Production,» *Available at SSRN,* vol. 435008, 2023.

[4] Y. Zhang, L. Pan, K. Pruess and S. Finsterle, “A time-convolution approach for modeling heat exchange between a wellbore and surrounding formation,” *Geothermics,* vol. 40, pp. 261-266, 2011.

[5] H. Carslaw and J. Jaeger, Conduction of Heat in Solids, 2nd ed., Oxford, UK: Oxford University Press, 1959, p. 334–339..

[6] J. R. Dormand and . P. J. Prince, “A family of embedded Runge-Kutta formulae,” *Journal of Computational and Applied Mathematics,* vol. 5, pp. 19-26, 1980.

[7] P. Virtanen, R. Gommers, T. Oliphant, M. Haberland, T. Reddy, D. Cournapeau, E. Burovski, P. Peterson, W. Weckesser, J. Bright, S. van der Walt, M. Brett, J. Wilson, K. Jarrod Millman, N. Mayorov, A. Nelson, E. Jones, R. Kern, E. Larson, C. Carey, I. Polat, Y. Feng, E. Moore, J. VanderPlas, D. Laxalde, J. Perktold, R. Cimrman, I. Henriksen, E. Quintero, C. Harris, A. Archibald, A. Ribeiro, F. Pedregosa, P. van Mulbregt and SciPy 1.0 Contributors, “SciPy 1.0: Fundamental Algorithms for Scientific Computing in Python,” *Nature Methods,* vol. 17, p. 261272, 2020.

[8] E. Lemmon, I. Bell, M. Huber and M. McLinden, “NIST Standard Reference Database 23: Reference Fluid Thermodynamic and Transport Properties-REFPROP, Version 10.0,” National Institute of Standards and Technology, Standard Reference Data Program, Gaithersburg, 2018.

[9] M. Bertini, D. Fiaschi, G. Manfrida, P. Niknam et T. Talluri, «Evaluation of the property methods for pure and mixture of CO2 for power cycles analysis,» *Energy Conversion and Management,* vol. 245, p. 114568, 2021.

[10] H. Ramey Jr., «Wellbore heat transmission,» *Journal of Petroleum Technology,* vol. 14, pp. 427-435, 1962.

[11] A. Al Saedi, R. Flori and C. Kabir, “New analytical solutions of wellbore fluid temperature profiles during drilling, circulating, and cementing operations,” *Journal of Petroleum Science and Engineering,* vol. 170, pp. 206-217, 2018.

[12] P. Sharma, A. Al Saedi and C. Kabir, “Geothermal energy extraction with wellbore heat exchanger: Analytical model and parameter evaluation to optimize heat recovery,” *Renewable Energy,* vol. 166, pp. 1-8, 2020.